ANL/NSE-20/12

Progress Report on the Assessment of the Material Performance for TCR Applications

Nuclear Science and Engineering Division

About Argonne National Laboratory
Argonne is a U.S. Department of Energy laboratory managed by UChicago Argonne, LLC under contract DE-AC02-06CH11357. The Laboratory's main facility is outside Chicago, at 9700 South Cass Avenue, Argonne, Illinois 60439. For information about Argonne and its pioneering science and technology programs, see www.anl.gov.

ANL/NSE-20/12

Progress Report on the Assessment of the Material Performance for TCR Applications

prepared by
Meimei Li, Xuan Zhang, Wei-Ying Chen, Florent Heidet
Nuclear Science and Engineering Division, Argonne National Laboratory

March 2020

Progress Report on the Assessment of the Material Performance for TCR Applications

Meimei Li, Xuan Zhang, Wei-Ying Chen, Florent Heidet
Nuclear Science and Engineering Division
Argonne National Laboratory

SUMMARY

The objective of Argonne's materials research activities for the Transformational Challenge Reactor (TCR) program is to improve the understanding of material properties from additive manufacturing with the focus on understanding the creep and fatigue properties of additively manufactured materials. The material work conducted by Argonne provides support in developing and qualifying advanced materials and manufacturing processes to allow for innovative reactor design and licensing for the TCR. In FY 2020, Oak Ridge National Laboratory (ORNL) provided six ASTM standard sized creep specimens of additively-manufactured 316L stainless steel (AM 316L SS) for evaluation of the effect of post-build heat treatment on the creep property. Two different teat treatments were conducted on the as-built specimens, namely 1050°C/1h and 650°C/1h before creep testing. All specimens were creep tested at 550°C and 275 MPa to understand the effect of heat treatments. We have also received AM 316L SS printed in various forms including rods and sheets, wrought 316 L SS (as a reference material), and AM IN718 for tensile, creep and fatigue testing. Both ASTM standard sized specimens and subsized specimens are being fabricated or tested to contribute to a comprehensive mechanical property database of AM materials and to provide location-specific property data to the TCR digital platform. Mechanical testing at Argonne is conducted to ASME NQA-1 or its lab equivalent for quality assurance.

This report presents the results of the creep tests at 550°C and microstructural characterization for the assessment of the effect of the post-build heat treatment on the creep behavior of AM 316L SS. It also discusses ongoing efforts on obtaining location-dependent properties of AM 316L SS.

PROGRESS AND STATUS

Introduction

Type 316 austenitic stainless steel is one of the most widely used structural materials in all types of nuclear reactors including current nuclear power plants and next-generation advanced nuclear reactor concepts, e.g. sodium-cooled fast reactors, molten-salt reactors, and gas-cooled very high temperature reactors. Additive manufacturing as a disruptive manufacturing technology has opened up unprecedented opportunities for designing next-generation advanced 316 SS components with controlled microstructure and enabling smart designs of reactor structural components with complex geometries, design freedom and possibly enhanced properties. Previous studies have shown that AM 316 SS has significantly improved yield and tensile strength combined with good ductility over conventionally-made wrought 316 SS at low temperatures [1-3]. The high-temperature mechanical performance of AM 316 SS is yet to be evaluated and fully understood. A comprehensive database of elevated temperature mechanical properties is needed

for its core structural applications in the TCR, a gas-cooled microreactor being developed to demonstrate revolutionary technologies including additive manufacturing [4,5]. Argonne's work has been focused on the evaluation and understanding of the creep and fatigue performance of additively manufactured materials.

Creep Property of AM 316L SS

Experimental

In FY 2019, we conducted six creep tests at 650°C using ASTM-standard round bar specimens (Fig. 1) of AM 316L SS provided by ORNL [6]. The specimens were fabricated from Build 20190308 printed by a laser powder bed fusion process using a Concept Laser–M2 printer [6]. Three of them were fabricated from rods printed in laser 1 mode (specimen IDs, L101, L102, L103), and the other three from rods printed in laser 2 mode (specimen ID, L201, L202, L203). This two-laser system enables direct one-to-one batch variability within a single build while keeping all other variables constant. The three specimens of laser 1 mode were creep tested at 650°C at 175, 200, and 225 MPa, respectively, and the three specimens of laser 2 mode were tested at the same temperature and stress conditions to evaluate the batch variability.

Six additional ASTM-standard round bar specimens were provided by ORNL in November 2019 (FY 2020) for the evaluation of the influence of post-build heat treatment on the creep property of AM 316L SS. These specimens were also fabricated from Build 20190308 rods with three of them in laser 1 mode (specimen IDs, L104, L105, L106), and the other three in laser 2 mode (specimen ID, L204, L205, L206). Post-build heat treatments were conducted at Argonne at 1050°C for one hour followed by rapid cooling on specimens L105 and L205, and at 650°C for one hour followed by furnace cooling on specimens L106 and L206, respectively. Each specimen was individually encapsulated in a quart tube under vacuum, and heat treated in an air furnace. Specimens L104 and L204 were in the as-built condition before creep tests. All specimens were creep tested under the same condition, namely, 550°C and 275 MPa. Table 1 provides a list of ASTM-standard creep specimens and testing conditions of AM 316L SS.

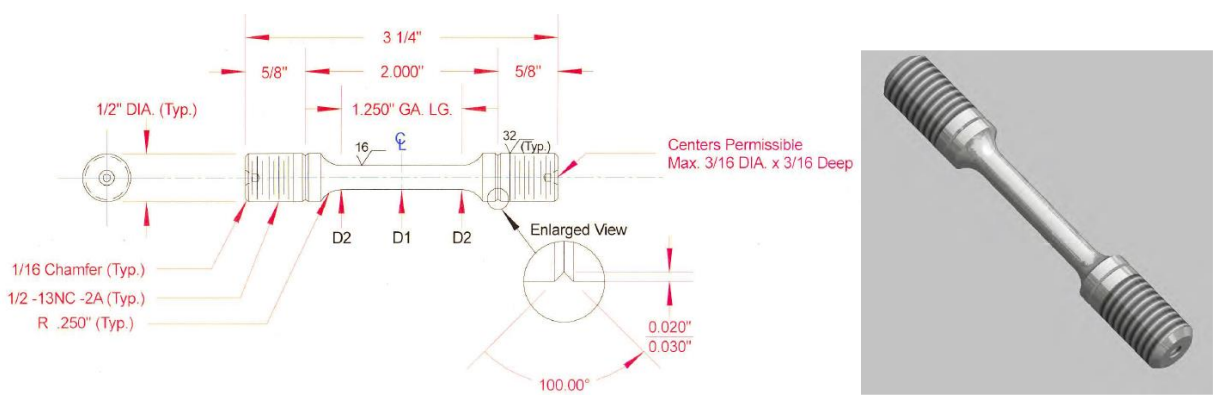

Figure 1. Schematic of ASTM-standard round bar creep specimens (unit: in).

Creep tests were conducted according to ASTM Standard E139-11, "Standard Test Methods for Conducting Creep, Creep-Rupture, and Stress-Rupture Tests on Metallic Materials." Tests were carried out on ATS Series 2300 Lever Arm Creep Testing Systems integrated with WinCCS II computer control and data acquisition software package (Fig. 2). Each creep frame is equipped with a three-zone split-tube furnace capable of operation up to 1100°C. An averaging extensometer frame was mounted on the specimen to measure the specimen displacement.

Table 1. List of ASTM-standard round bar creep specimens and test conditions of AM 316 L SS.

Specimen ID	Build ID	Laser mode	Specimen Type	Condition	Test T (°C)	Stress (MPa)	Environ.
L101	20190308	Laser 1	ASTM	As-built	650	225	Air
L102	20190308	Laser 1	ASTM	As-built	650	200	Air
L103	20190308	Laser 1	ASTM	As-built	650	175	Air
L104	20190308	Laser 1	ASTM	As-built	550	275	Air
L105	20190308	Laser 1	ASTM	1050°C/1h	550	*	Air
L106	20190308	Laser 1	ASTM	650°C/1h	550	275	Air
L201	20190308	Laser 2	ASTM	As-built	650	225	Air
L202	20190308	Laser 2	ASTM	As-built	650	200	Air
L203	20190308	Laser 2	ASTM	As-built	650	175	Air
L204	20190308	Laser 2	ASTM	As-built	550	275	Air
L205	20190308	Laser 2	ASTM	1050°C/1h	550	275	Air
L206	20190308	Laser 2	ASTM	650°C/1h	550	275	Air

*L105 failed at 550°C during initial loading to 375 MPa. The applied creep stress was then reduced to 275 MPa for other five specimens.

Figure 2. Argonne's creep test systems.

Results

The 650°C creep data of AM 316L SS was presented in a previous report [6]. In summary, specimens in laser 1 and laser 2 modes showed comparable creep behavior. AM 316L SS showed a very short steady-state creep, compared with conventional Type 316 SS. The minimum creep rate was reached in the first few hours followed by a continuous increase in creep rate to the final failure. The minimum creep rate of AM 316L SS followed a power law relationship with the applied stress, $\dot{\varepsilon} = A\sigma^n$, with the power exponent of n = 12, which implies a low-temperature dislocation creep mechanism.

Figure 3 shows the creep strain as a function of time for the five creep specimens tested at 550°C and 275 MPa to evaluate the influence of the post-build heat treatment on creep properties. L105 failed at 550°C during initial loading to 375 MPa. The applied stress was reduced for other five specimens, and they were tested at 550°C and 275 MPa. The creep rupture data are given in Fig. 4. Post-build heat treatment of 1050°C/1h significantly reduced the creep life, while the heat treatment of 650°C/1h slightly increased the creep life compared with the creep life of the as-built specimen. Specimens of laser 1 mode (L104 and L106) showed somewhat longer creep lives than specimens of laser 2 mode (L204 and L206). The as-built specimens and the 650°C/1h heat treated specimens had a very short steady-state stage (a few percent of the total life) followed by an accelerated creep until the final failure, similar to the observations of the 650°C creep tests. The 1050°C/1h heat treated specimen had a much more pronounced steady-state creep, resembling the creep behavior of conventional 316 SSs. The minimum creep rate of the 1050°C/1h heat treated specimen is about six times higher than the minimum creep rates of all other specimens, as shown in Fig. 5. The minimum creep rates of the 650°C/1h heat treated specimens are smaller than those of the as-built specimens. Specimens of laser 1 mode have somewhat lower creep rates than specimens of laser 2 mode. Figure 6 shows that all the specimens exhibited slant fracture.

The creep property data of AM 316L SS at 550 and 650°C are summarized in Table 2. Figure 7 shows the creep rupture data of AM 316L SS at 550 and 650°C and compares the 550°C data with the creep rupture equation at 550°C for conventional 316 SS developed by ORNL [7]. It is shown that AM 316L SS has a shorter creep life than Type 316 SS regardless of the AM specimen condition. Post-build heat treatment of 650°C/1h improved the creep rupture life of AM 316L, which is still below that for conventional 316 SS. Post-build solution annealing treatment of 1050°C/1h significantly shorten the creep life. Figure 8 summarizes the minimum creep rate data for AM 316L SS at 550 and 650°C. Creep data obtained up to date show that the batch variability between laser 1 and laser 2 modes is insignificant.

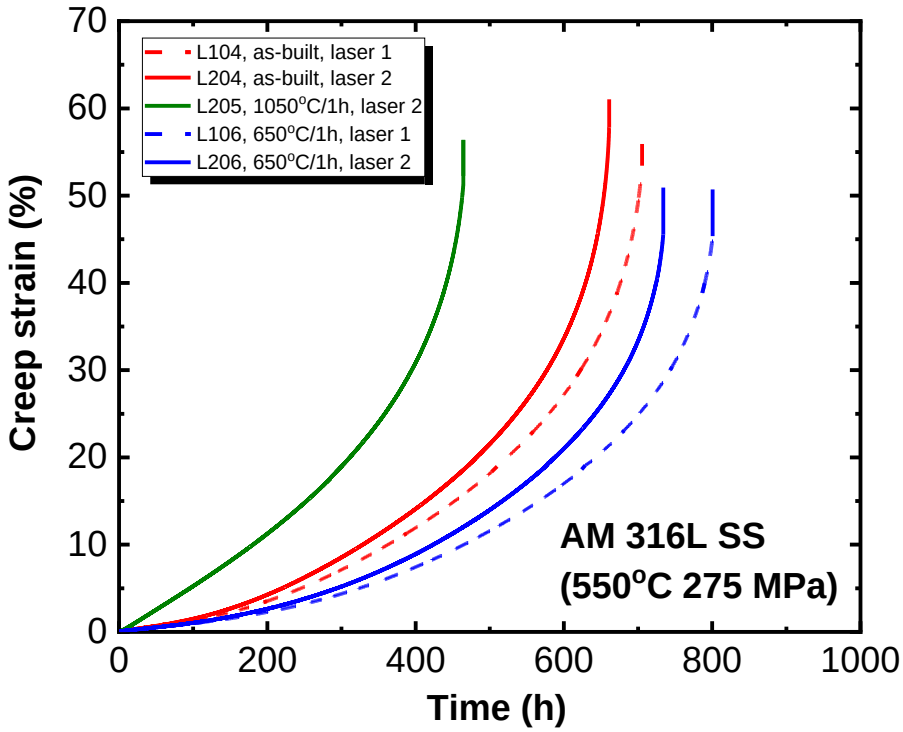

Figure 3. Creep strain as a function of time for AM 316L SS tested at 550°C and 275 MPa.

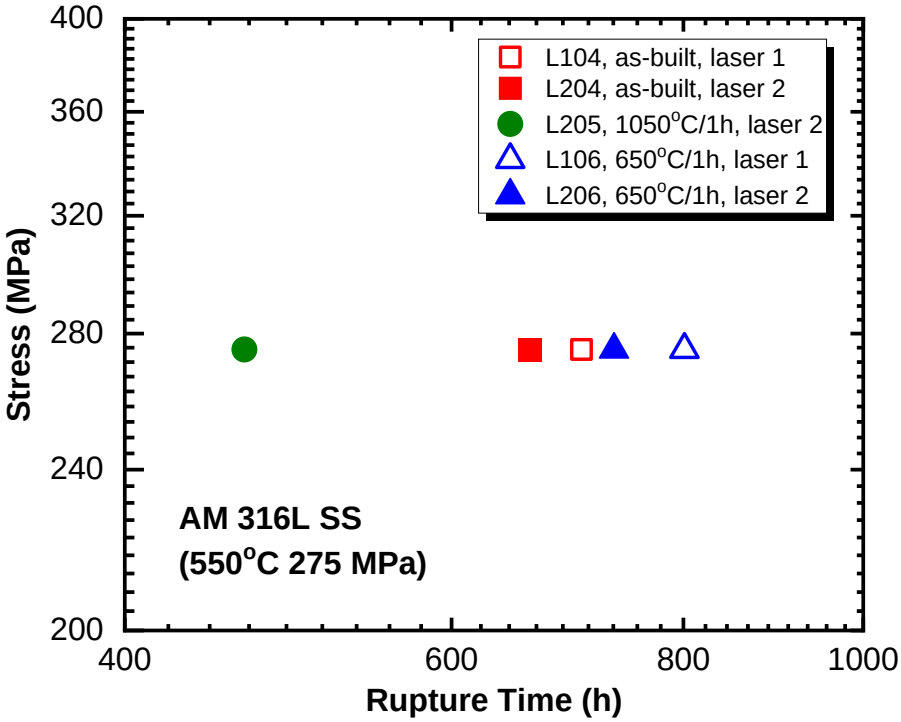

Figure 4. Creep rupture data for AM 316L SS tested at 550°C and 275 MPa.

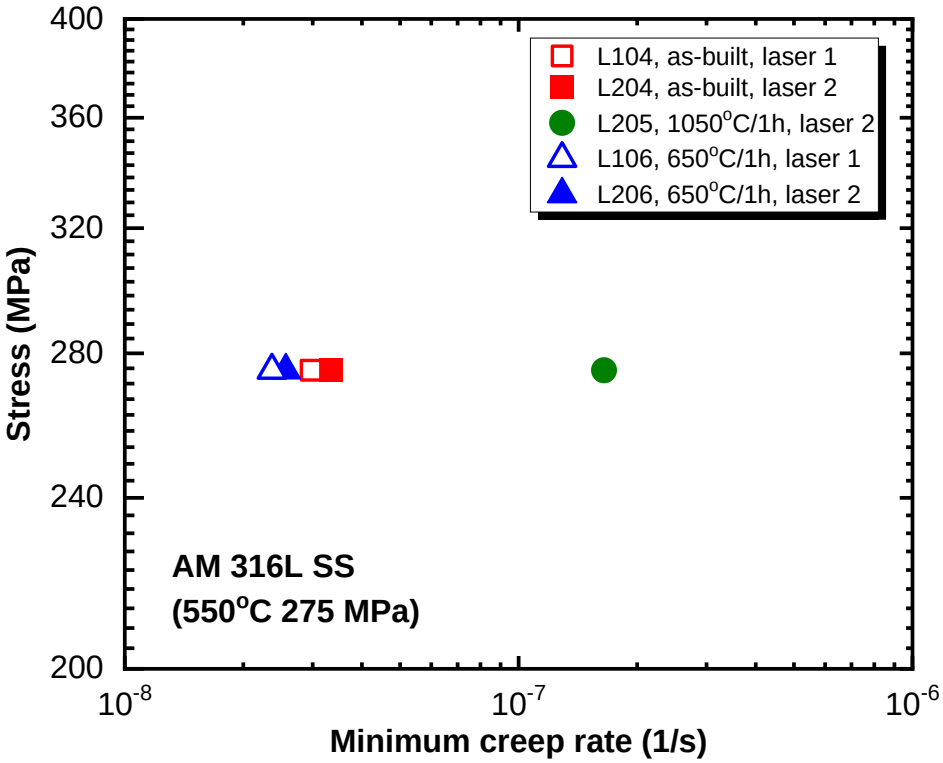

Figure 5. Minimum creep strain rates for AM 316L SS tested at 550°C and 275 MPa.

Figure 6. Photographs of the AM 316L SS creep-ruptured specimens.

Table 2. Creep property data of AM 316 L SS tested at 550 and 650°C.

Specimen ID	Laser mode	Condition	Test Temp (°C)	Stress (MPa)	Rupture time (h)	Minimum Creep rate (1/s)	Creep rupture strain (%)	R.A. (%)
L101	Laser 1	As-built	650	225	13.8	1.22×10^{-6}	46.9	45.1
L102	Laser 1	As-built	650	200	41.6	2.59×10^{-7}	40.7	43.0
L103	Laser 1	As-built	650	175	150.3	6.41×10^{-8}	45.8	44.2
L104	Laser 1	As-built	550	275	705.4	2.97×10^{-8}	55.9	53.5
L106	Laser 1	650°C/1h	550	275	800.6	2.36×10^{-8}	50.7	53.4
L201	Laser 2	As-built	650	225	13.0	1.39×10^{-6}	47.5	46.0
L202	Laser 2	As-built	650	200	43.9	2.53×10^{-7}	53.5	46.9
L203	Laser 2	As-built	650	175	144.5	6.61×10^{-8}	43.2	44.2
L204	Laser 2	As-built	550	275	661.0	3.33×10^{-8}	61.0	58.1
L205	Laser 2	1050°C/1h	550	275	464.4	1.65×10^{-7}	56.4	54.7
L206	Laser 2	650°C/1h	550	275	734.0	2.56×10^{-8}	50.9	57.7

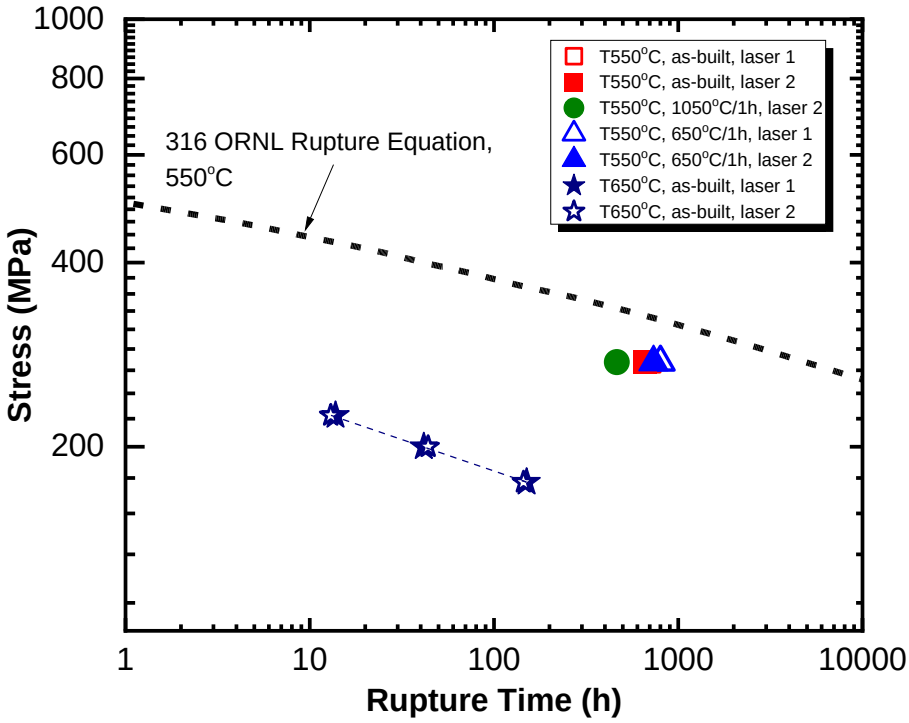

Figure 7. Creep rupture data for AM 316L SS tested at 550 and 650°C and comparison with the 316 ORNL rupture equation (550°C) [7].

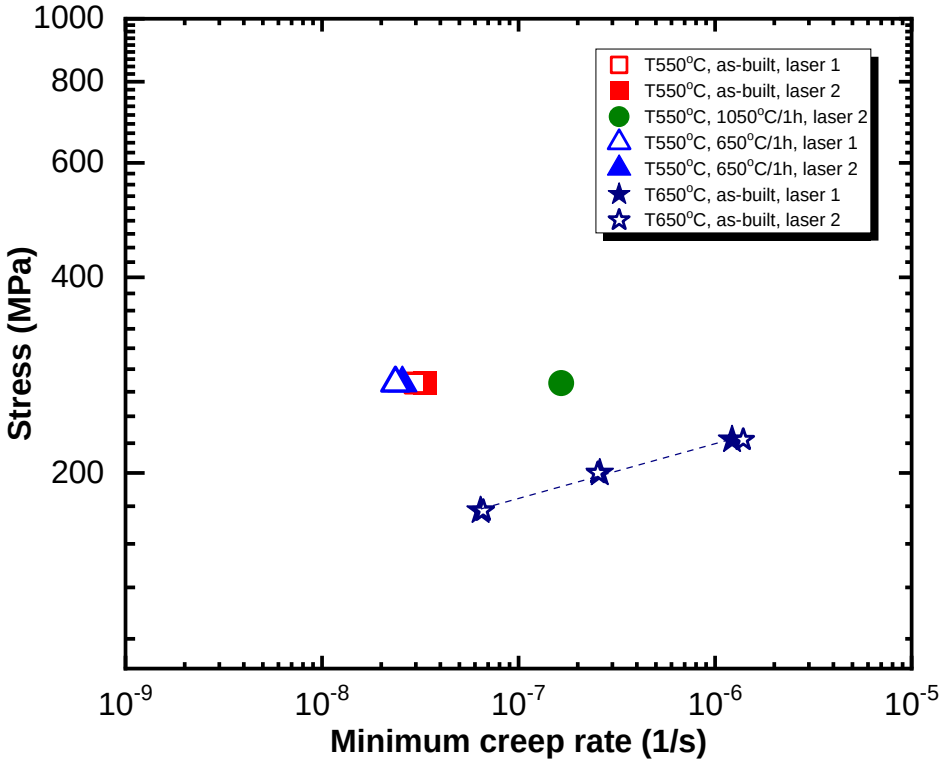

Figure 8. Minimum creep strain rates for AM 316L SS tested at 550 and 650°C.

Microstructure of AM 316L SS

To examine the microstructure of the as-built AM 316L SS, a thin sheet (~0.25 mm thick) was sectioned from a rod (laser 1 mode, 20190308 build) approximately 0.7" away from an end of the rod. Disk specimens of 3 mm in diameter were made from the thin sheet for transmission electron microscopy (TEM). TEM disk specimens were electropolished to perforation using an electrolyte of 5% methanol and 95% perchloric acid at ~-40°C.

TEM images at various magnifications in Fig. 9 reveal well-organized dislocation cells in the as-built AM 316L SS. The cell size is ~ 500 nm. The dislocation density is very low inside cells. Both cell boundaries and grain boundaries are decorated with precipitate particles. EDS elemental mapping shows that the particles are oxides enriched in Si, Mn; elemental segregation was observed at cell boundaries which are enriched in Cr and Mo and depleted of Fe, as shown in Fig. 10. The observations are consistent with the findings reported in the literature, e.g. [8].

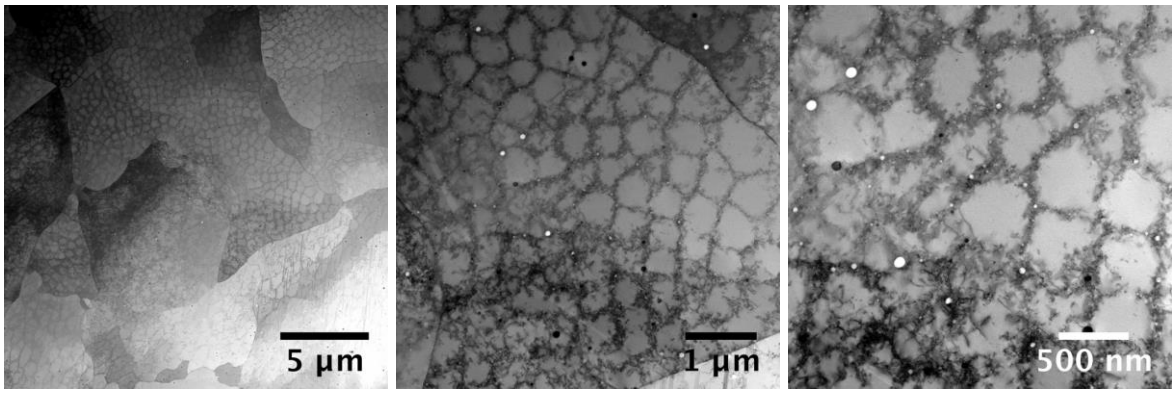

Figure 9. TEM micrographs showing the microstructure of the as-built AM 316 L SS (Laser 1 Build 20190308).

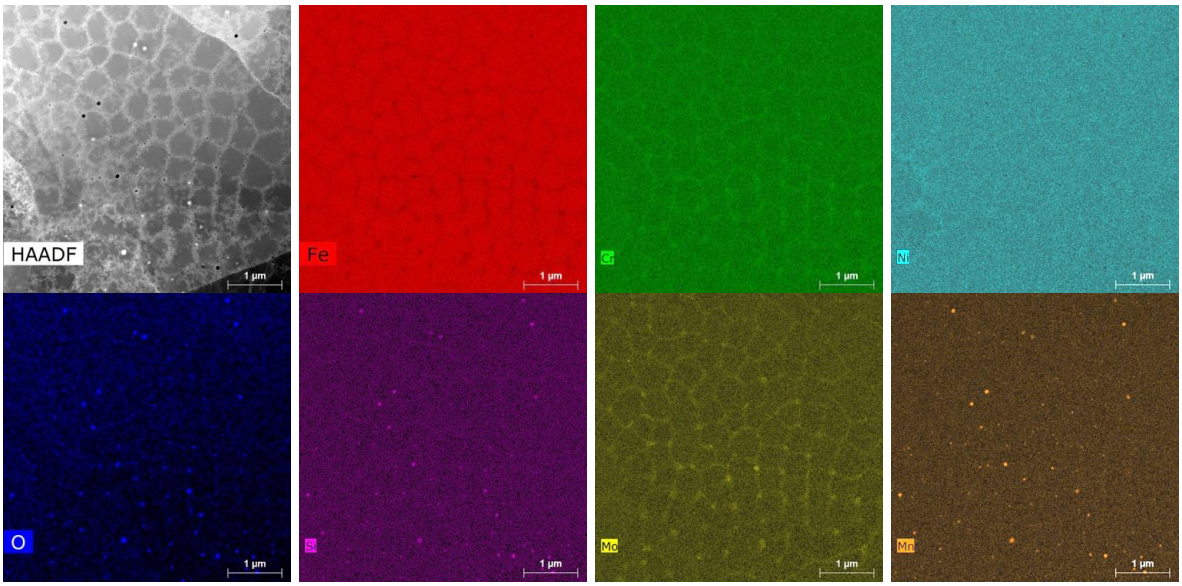

Figure 10. HAADF micrograph and EDS elemental maps of the as-built AM 316 L SS.

Heat treatment at 1050°C/1h effectively removed the dislocation cell structure and elemental segregation at cell boundaries observed in the as-built condition, as shown in Figs. 11 and 12. Note that TEM disk specimens were taken from the grip section of specimen L205 who experienced an additional thermal exposure of 550°C for 464 h during the creep test. This thermal exposure is expected to have an insignificant effect on TEM-visible microstructure. Unlike conventional solution-annealed Type 316 SS, dislocation lines and precipitates were observed within equiaxed grains after the heat treatment of 1050°C/1h in AM 316L SS. EDS elemental mapping (Fig. 12) shows oxide particles enriched in Cr and Mn, which have different chemistry from those observed in the as-built condition (Fig. 10). The particle size in the 1050°C/1h heat treated specimen is significantly larger, with the mean size of 87 nm relative to the particle mean size of 25 nm in the as-built specimen (Fig. 13). It is also noted that particles in the as-built specimen appear to have a bimodal size distribution.

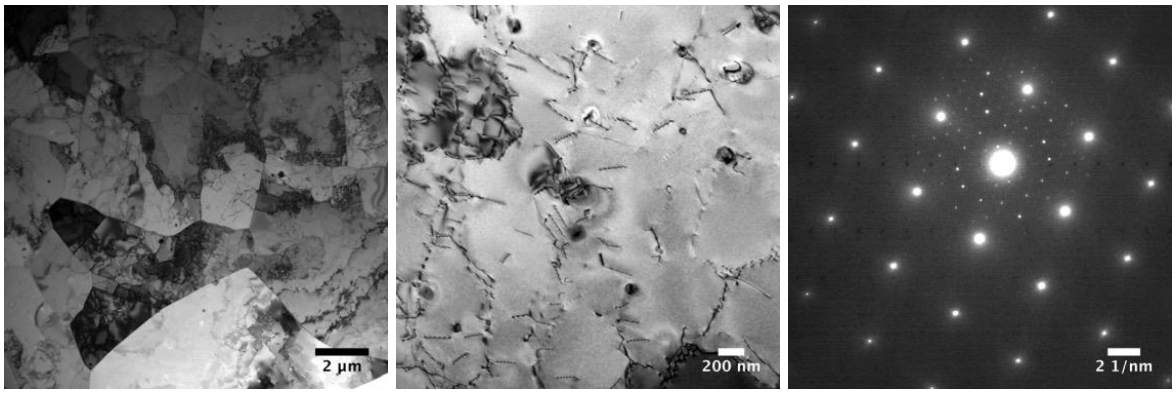

Figure 11. TEM micrographs showing the microstructure of the AM 316 L SS heat treated at 1050°C/1h. The TEM specimen was taken from the grip section of specimen L205.

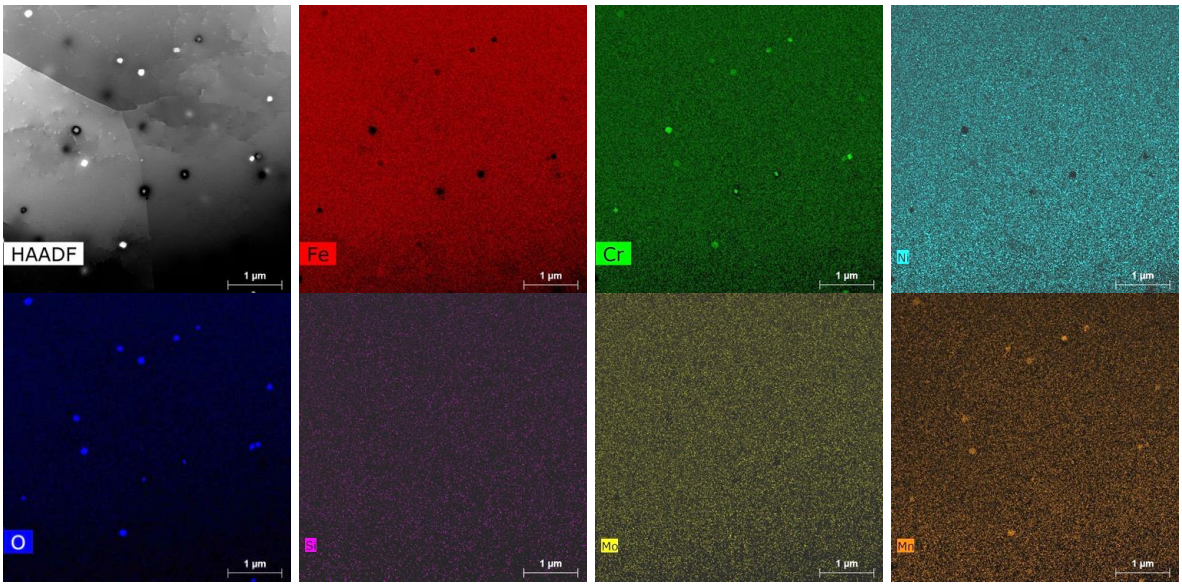

Figure 12. HAADF micrograph and EDS elemental maps of the AM 316 L SS heat treated at 1050°C/1h. The TEM specimen was taken from the grip section of specimen L205.

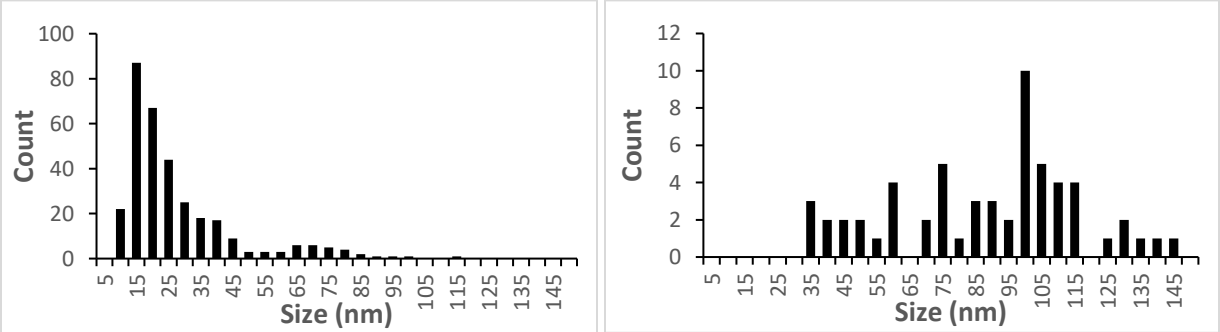

Figure 13. Particle size distributions in the as-built condition (mean size = 25 nm) (left) and in the 1050°C/1h heat treated condition (mean size = 87 nm) (right).

TEM disk specimens were cut from the gauge section of specimens after creep tests to examine the microstructural change during creep deformation. Electropolishing of TEM disks was a challenge due to the presence of cracks, voids, or porosity. Electropolished thin foil specimens were further ion milled to obtain appreciable thin areas for TEM observations.

Figure 14 shows the microstructure of the as-built AM 316L SS after the creep test at 550°C/275 MPa. Specimen was taken from the gauge of specimen L204. It was found that the initial dislocation cells mostly evolved into dislocation tangles with some cell structures still observable but less well defined. A similar observation was made in the 650°C/1h heat treated specimen after the creep test, i.e. heavy dislocation tangles, but the cell structure was not evident, as shown in Fig. 15 (TEM specimen was taken from the gauge section of specimen L206). The through-focus imaging reveal features with lower electron density features in some of the grains, segregated along dislocation lines. These features are possibly voids or precipitates, and their exact nature is to be resolved. High density of dislocations was also observed in the 1050°C/1h heat treated specimen after the creep test, as shown in Fig. 16. It appears that the end microstructure after the creep test was similar regardless of the initial state.

Fast cooling rates during the laser powder bed fusion process can produce highly non-equilibrium microstructure and high residual stress. Post-build heat treatment of 650°C/1h can potentially reduce the residual stress in the as-built condition. The solution annealing treatment at 1050°C/1h removed the dislocation cell structure and elemental segregation at boundaries, resulting in equilibrium structure and homogeneous solute distribution. The oxide particles in the as-built condition, (Mn,Si)O were replaced with oxides, (Mn,Cr)O, potentially more stable in equilibrium, and Si atoms dissolved in the solution. It is suggested that the dislocation cell structure in the as-built condition is largely responsible for the observed low minimum creep rate. This structure is however unstable, and can readily undergo dynamic recovery during creep, resulting in an accelerated creep. The oxide particles distributed along the cell boundaries may also play a role in reducing the creep rate and slow the recrystallization process during the post-build solution annealing treatment.

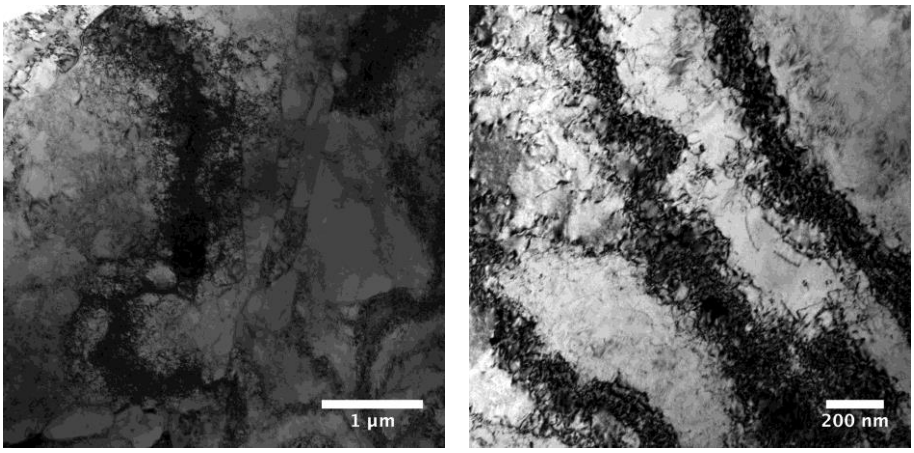

Figure 14. TEM micrographs showing the microstructure of the as-built AM 316 L SS after creep test at 550°C/275 MPa. TEM specimen was taken from the gauge section of specimen L204.

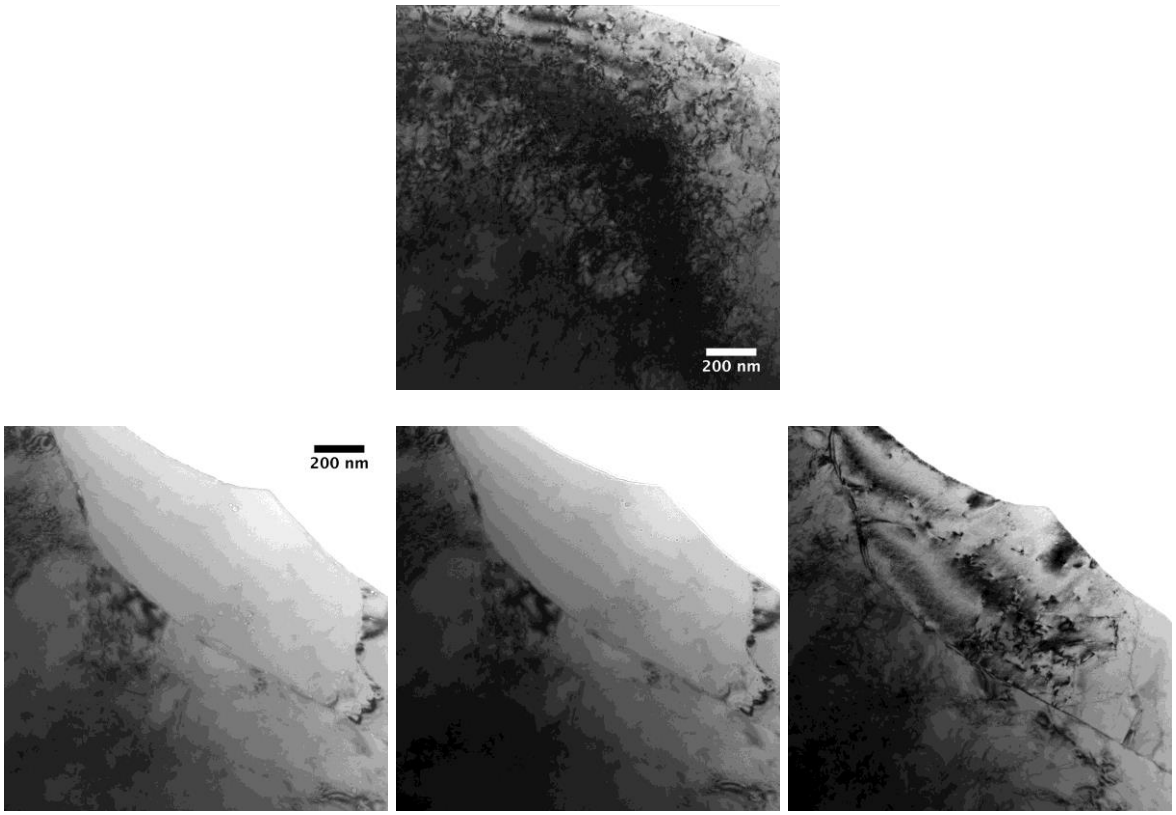

Under-focus Over-focus In-focus

Figure 15. TEM micrographs showing the microstructure of the 650°C/1h heat treated AM 316 L SS after creep test at 550°C/275 MPa. The under-focus, over-focus, and in-focus images show voids or precipitates inside a grain. TEM specimen was taken from the gauge section of specimen L206.

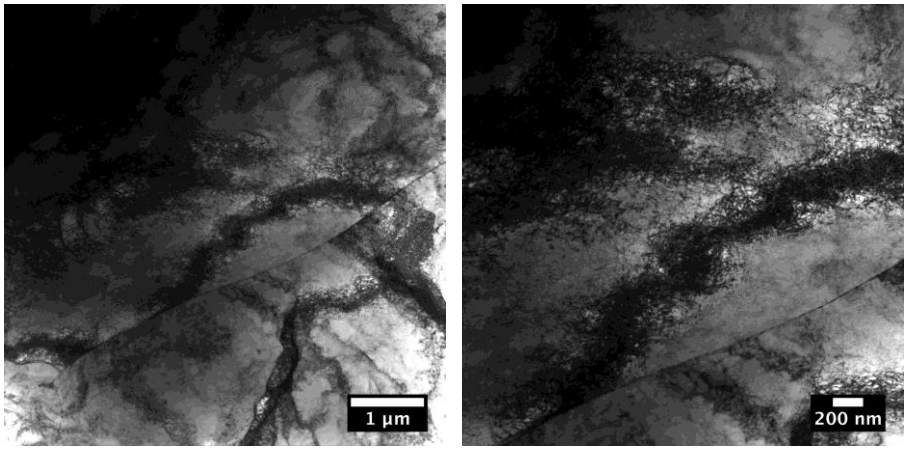

Figure 16. TEM micrographs showing the microstructure of the 1050°C/1h heat treated AM 316 L SS after creep test at 550°C/275 MPa. TEM specimen was taken from the gauge of specimen L205.

Location-Dependent Tensile Properties of AM 316L SS

To evaluate the effect of part geometry on tensile and creep properties and to provide location-specific data to the TCR digital platform, 24 subsized SS-3 sheet-type specimens per rod were EDM-machined from rod L1-8 and L2-8, respectively of AM 316L SS provided by ORNL. Rod L1-8 was printed in laser 1 mode and rod L2-8 printed in lase 2 mode with the build ID of 20190315. The nominal diameter and length of the rods are 0.5”×4.2”. The nominal gauge dimensions of the SS-3 specimen are 0.300”×0.060”×0.035”. The specimens were oriented with the gauge in parallel with the build direction, and three rows of specimens were machined along the build direction with each row having eight specimens and four each symmetrically situated from the centerline of the cross section of the rod, as shown in Fig. 17. To track the location of each specimen, the length of the upper grip section of the specimen was increased by different amounts relative to the length of the lower grip section (instead of equal lengths as in a conventional specimen). Specifically, the upper grip is 0.09” longer than the lower grip in the top row specimens, 0.06” longer in the middle row specimens, and 0.03” longer in the bottom row specimens. The location of a specimen within a rod is also tracked by the specimen ID. For example, the ID “1T1” has the first number “1” representing laser 1 mode, the second letter “T” representing the top section of the rod, and the third letter “1” showing the location of the specimen in the cross section of the rod (see the cross section view in Fig. 17).

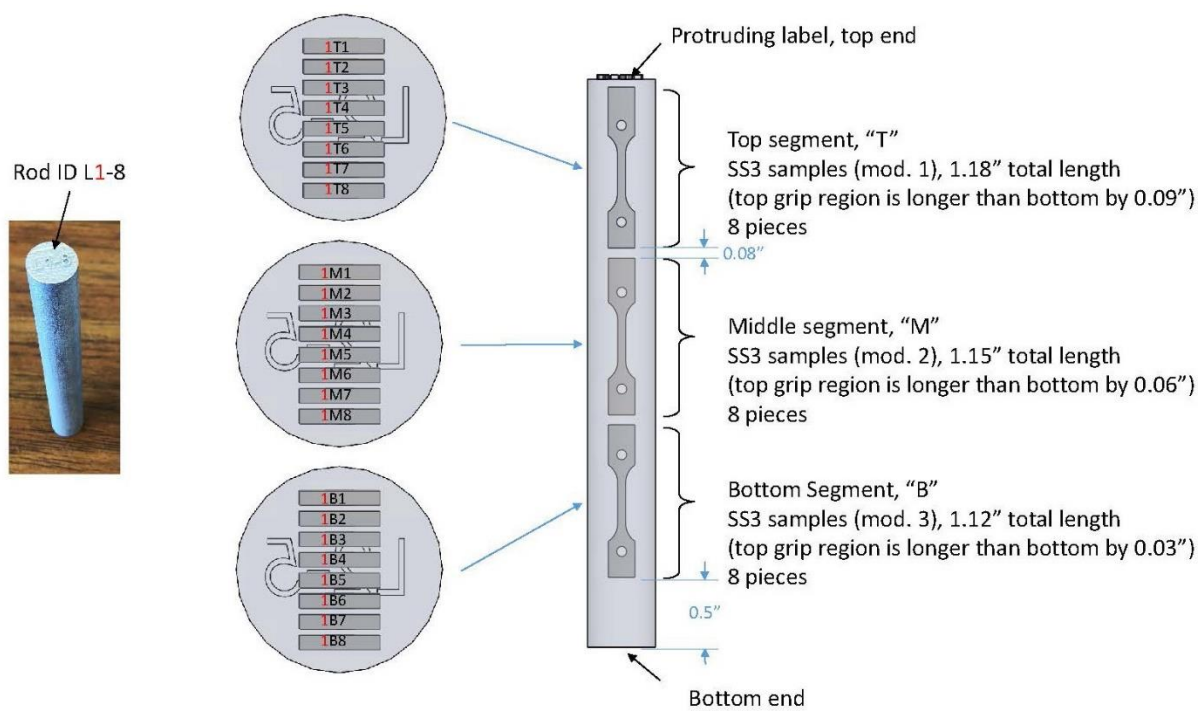

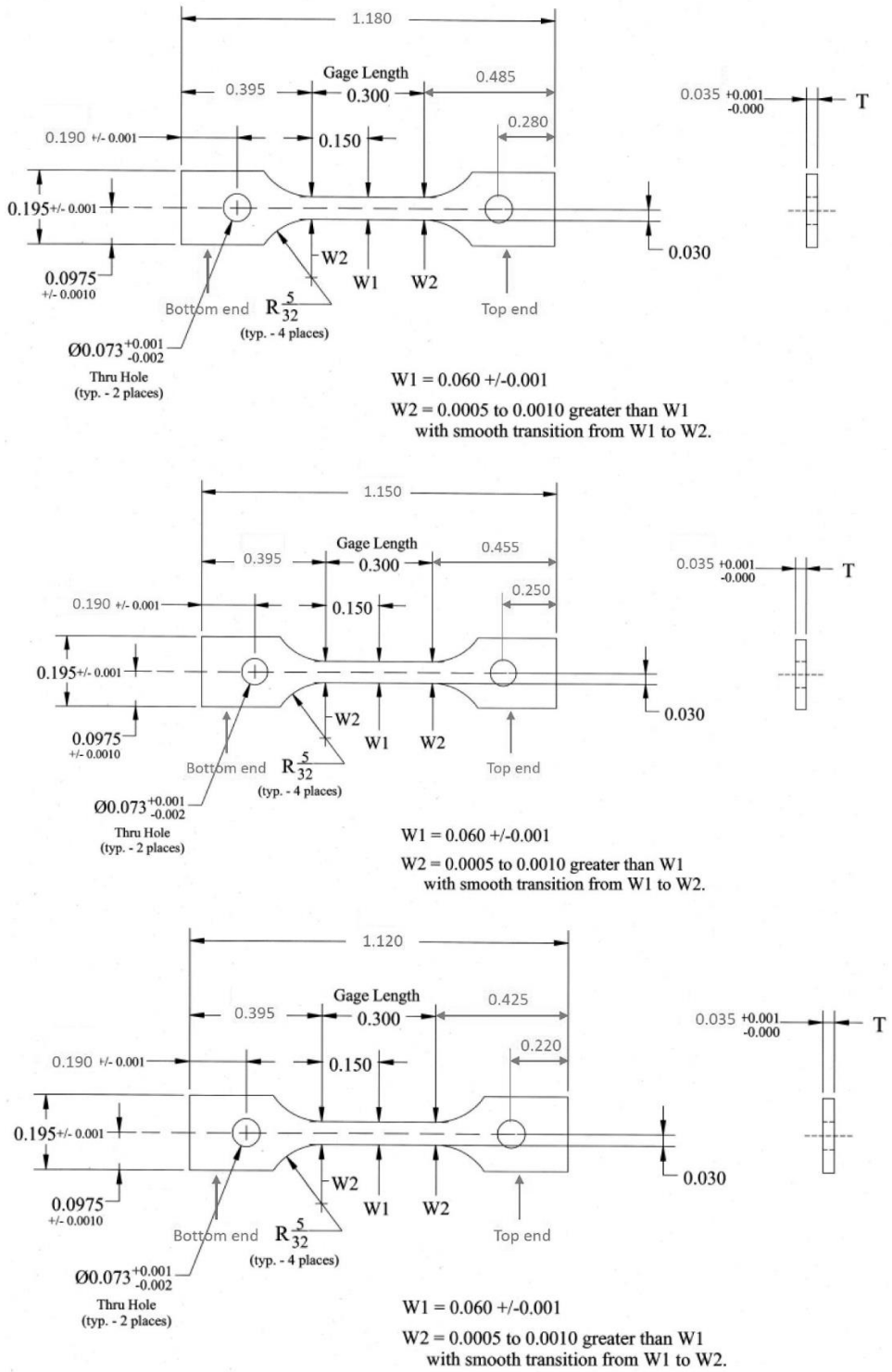

Figure 17. Specimen fabrication drawing showing the orientation and location of each specimen and schematic drawings of SS-3 sheet-type tensile specimens in the top, middle, and bottom sections of the printed rod (unit: in).

Tensile tests were performed in an electromechanical testing system equipped with the Instron Bluehill software. Tests were conducted at 550°C at a nominal strain rate of 1×10^{-3}/s using a set of pin-loading grips. The applied load was recorded by a load cell; the specimen displacement was measured by the crosshead extension. The engineering tensile properties were determined from the analysis of the load and displacement data.

Figure 18 shows the engineering stress-strain curves of four specimens: two in the top section and the other two in the bottom section of rod L1-8. These four specimens showed remarkably similar tensile behavior with comparable yield stress (YS), working hardening rate, and ultimate tensile strength (UTS). Their tensile ductility, however, varied: specimen 1B4 has the lowest uniform elongation (UE) and total elongation (TE), and specimen 1T4 has the highest elongations, and both specimens are close to the centerline of the rod. Specimens 1B2 and 1T2, which are close to the periphery of the rod, have similar elongation values that are between the elongation values of specimens 1B4 and 1T4. There appears to be a location-dependence of tensile ductility, as illustrated in Fig. 19. Specimens in the middle section of rod L1-8 will be tested to provide further information. The tensile properties including yield stress, ultimate tensile strength, uniform and total elongations are summarized in Table 3.

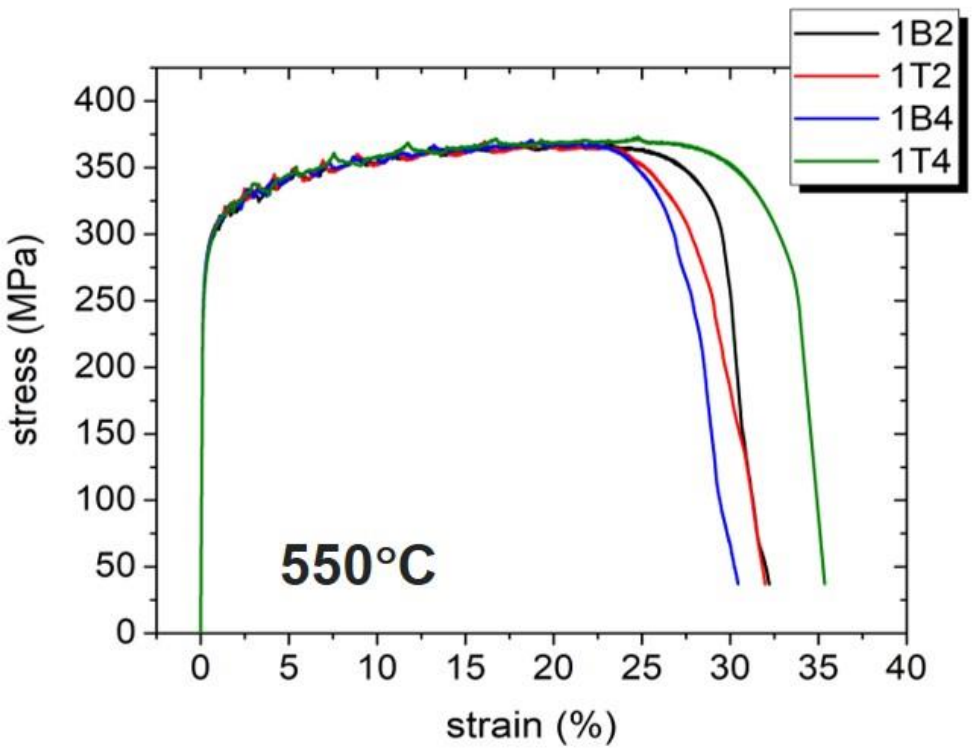

Figure 18. Engineering stress-strain curves at 550°C for specimens taken in the top and bottom sections of rod L1-8.

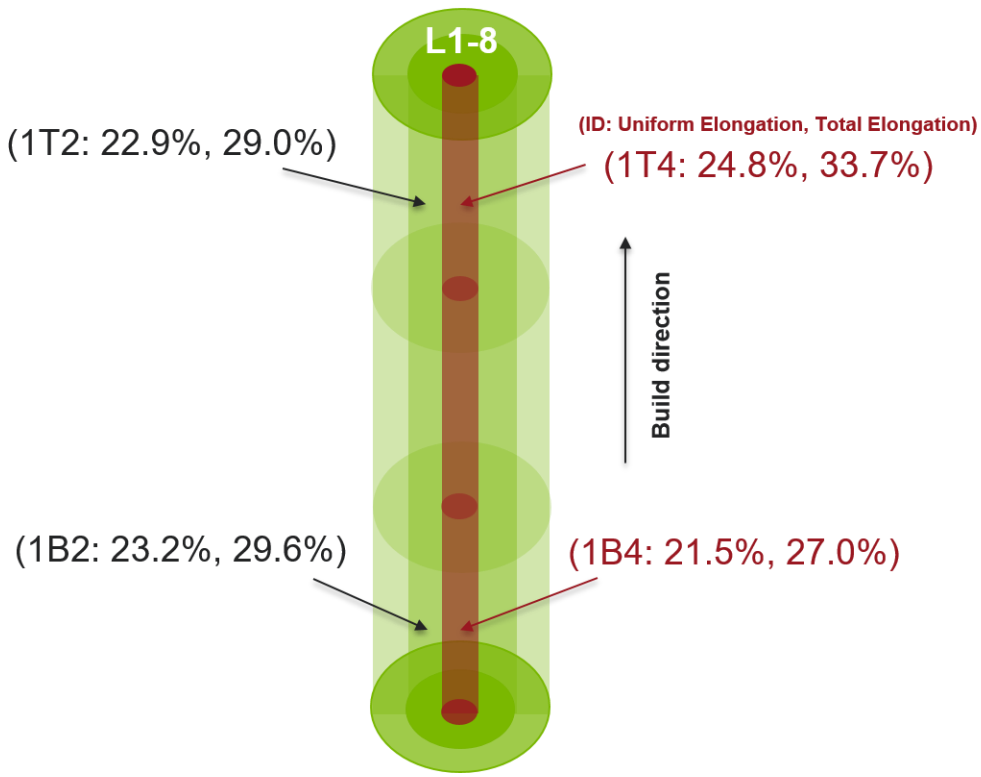

Figure 19. Illustration of location-dependent uniform and total elongation values in the printed rod L1-8. Tensile tests were conducted at 550°C.

Table 3. Location-dependent tensile property data of AM 316 L SS.

Specimen ID	Rod ID	Specimen Type	Test T (°C)	Strain rate (1/s)	YS (MPa)	UTS (MPa)	UE (%)	TE (%)
1T2	L1-8	SS-3	550	0.001	281	370	22.9	29.0
1T4	L1-8	SS-3	550	0.001	277	373	24.8	33.7
1B2	L1-8	SS-3	550	0.001	277	368	23.2	29.6
1B4	L1-8	SS-3	550	0.001	281	371	21.5	27.0

FUTURE WORK

Work on location-dependent tensile property will continue. Tensile tests at different temperatures and at lower strain rates are planned. Location-specific creep property data will also be produced using subsized SS-3 specimens. Four ASTM standard size round bar creep specimens in laser mode 1 and laser mode 2, respectively and three ASTM standard size round bar creep specimens in laser mode 1 and laser mode 2, respectively were fabricated from printed rods and

are ready to be tested. Creep and low-cycle fatigue tests at 550 and 600°C have been planned for these specimens.

We have recently received materials from ORNL including a new build of AM 316L SS, wrought 316L SS, and AM IN718. Subsized specimens will be fabricated from the materials and will be used for the evaluation of tensile, creep and fatigue properties.

ACKNOWLEDGEMENT

Work was supported by the Transformational Challenge Reactor Program funded by the U.S. Department of Energy, Office of Nuclear Energy under Contract DE-AC02-06CH11357. Materials were provided by Oak Ridge National Laboratory. Use of the Center for Nanoscale Materials, an Office of Science user facility, was supported by the U.S. Department of Energy, Office of Science, Office of Basic Energy Sciences, under Contract No. DE-AC02-06CH11357. We would like to thank Ed Listwan, Joe Listwan and David Rink for assistance of tensile and creep tests.

REFERENCES

1. Z. Sun, X. Tan, S.B. Tor, C. K. Chua, “Simultaneously enhanced strength and ductility for 3D-printed stainless steel 316L by selective laser melting,” NPG Asia Materials 10 (2018) 127.
2. Y.M. Wang, T. Voisin, J.T. McKeown, J. Ye, N.P. Calta, Z. Li, Z.Zeng, et al., “Additively manufactured hierarchical stainless steels with high strength and ductility”, Nature Materials 17 (2018) 63.
3. G.T. Gray III, V. Livescu, P.A. Rigg, C.P. Trujillo, C.M. Cady, S.R. Chen, J.S. Carpenter, T.J. Lienert, S.J. Fensin, “Structure/property (constitutive and spallation response) of additively manufactured 316L stainless steel”, Acta Materialia 138 (2017) 140.
4. Oak Ridge National Laboratory. "Transformational Challenge Reactor," Oak Ridge National Laboratory. https://tcr.ornl.gov/.
5. J. Simpson, J. Haley, C. Cramer, O. Shafer, A. Elliott, W. Peter, L. Lover, R. Dehoff, “Considerations for application of additive manufacturing to nuclear reactor core components,” ORNL/TM-2019-1190, Oak Ridge National Laboratory (2019).
6. K.G. Field, J. Simpson, M.N. Gussev, H. Wang, M. Li, X. Chen, T. Koyanagi, K. Kane, A.M. Rossy, M. Balooch, K.A. Terrni, “Handbook of advanced manufactured material properties from TCR structure builds at ORNL – FY19,” ORNL/TM-2019/1328 (2019).
7. C. R. Brinkman, “Elevated-temperature mechanical properties of an advanced Type 316 stainless steel,” ORNL/CP-101053.
8. S. Li, J. Ju, W. Chen, J. Yu, M. Li, Y. Wang, “Evolution of cellular dislocation structures and defects in additively manufactured austenitic stainless steel under ion irradiation,” Script Mater. 178 (2020) 245.

Nuclear Science and Engineering Division
Argonne National Laboratory
9700 South Cass Avenue, Bldg. 401
Argonne, IL 60439

www.anl.gov

Argonne National Laboratory is a U.S. Department of Energy
laboratory managed by UChicago Argonne, LLC